Instabilities of nontrivial-phase solutions of the cubic Nonlinear Schrödinger equation

Draft - August 16, 2005

Abstract

We consider the two dimensional cubic Nonlinear Schrödinger (NLS) equation, which admits a large family of one-dimensional traveling wave solutions. All such bounded solutions may be written in terms of an amplitude and a phase. If the phase of this solution is dependent on the spatial dimension of the one-dimensional wave form, this solution is refered to as having nontrivial phase (NTP). We study the spectral stability analysis of such NTP solutions numerically, using a extension of Hill's method. We present evidence which suggests that all such NTP solutions are unstable with respect to transverse perturbations. This transverse instability occurs in both the elliptic and hyperbolic NLS equations, and in the focusing and defocusing case.

1 Introduction

The cubic Nonlinear Schrödinger (NLS) equation in two spatial dimensions is given by

$$i\psi_t + \alpha\psi_{xx} + \beta\psi_{yy} + |\psi|^2\psi = 0. \tag{1}$$

This equation admits a large family of one-dimensional traveling wave solutions. These solutions may be written in the form

$$\psi(x,t) = \phi(x)e^{i\theta(x)+i\lambda t}, \tag{2}$$

where $\phi(x)$ and $\theta(x)$ are real-valued functions, and λ is a real constant. Bounded solutions of the form (2) are possible if

$$\phi^2(x) = \alpha\left(-2k^2\,\mathrm{sn}^2(x,k) + B\right), \tag{3a}$$
$$\theta(x) = c\int_0^x \phi^{-2}(\xi)d\xi, \tag{3b}$$
$$\lambda = \tfrac{1}{2}\alpha(3B - 2(1+k^2)), \qquad \text{and} \tag{3c}$$
$$c^2 = -\tfrac{\alpha^2}{2}B(B-2k^2)(B-2), \tag{3d}$$

with c real. Here $k \in [0,1]$ is the elliptic modulus of the Jacobi elliptic sine function, $\mathrm{sn}\,(x,k)$. The function $\mathrm{sn}\,(x,k)$ is periodic, with period given by $L = 4K$, with

$$K(k) = \int_0^{\pi/2} \left(1 - k^2\sin^2 x\right)^{-1/2}\, dx,$$

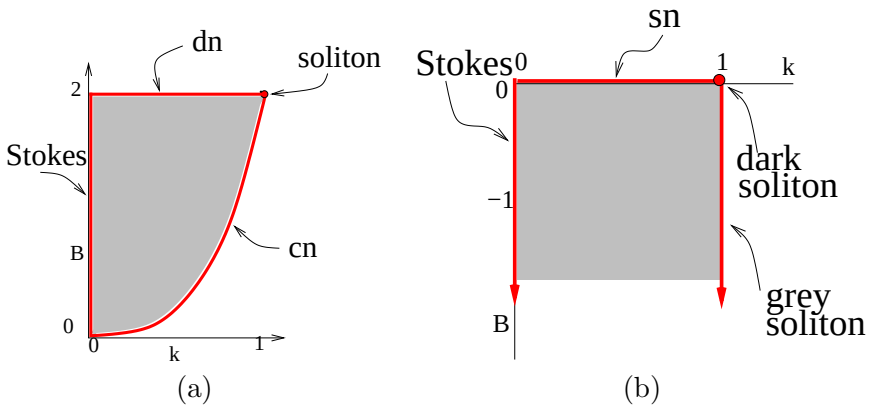

Figure 1: Admissible parameter space for (a) focusing ($\alpha = 1$) and (b) defocusing ($\alpha = -1$) regimes

TP	ψ	NTP ($\alpha = -1$)	NTP ($\alpha = 1$)
Stokes		$k = 0, B \leq 0$	$k = 0, 0 \leq B \leq 2$
cn	$\pm\sqrt{2\alpha}k\,\mathrm{cn}\,(x,k)e^{i\alpha(2k^2-1)t}$	N/A	$0 \leq k < 1, B = 2k^2$
dn	$\pm\sqrt{2\alpha}k\,\mathrm{dn}\,(x,k)e^{i\alpha(2-k^2)t}$	N/A	$0 \leq k < 1, B = 2$
sn	$\pm\sqrt{-2\alpha}k\,\mathrm{sn}\,(x,k)e^{-i\alpha(1+k^2)t}$	$0 \leq k < 1, B = 0$	N/A
soliton	$\pm\sqrt{2\alpha}\mathrm{sech}(x)e^{i\alpha t}$ $\pm\sqrt{2\alpha}\tanh(x)e^{2i\alpha t+B}$?	Grey $k = 1, B <= 0$	Bright $k = 1, B = 2$

Table 1: I need to work on this table still. Parameter values which reduce the NTP solutions to simpler solutions.

the complete elliptic integral of the first kind [3]. When $k = 0$, $\mathrm{sn}\,(x,0) = \sin(x)$ with $L = 2\pi$. As k approaches 1, $\mathrm{sn}\,(x,k) \longrightarrow \tanh(x)$ as $L \longrightarrow$ infinity.

The solution ψ is said to have *trivial phase* (TP) if $\theta(x)$ is constant and *nontrivial phase* (NTP) if $\theta(x)$ is not constant. For every choice of α and β, (3) specifies a 2-parameter family of solutions with free paramters k and B. Without loss of generality, both α and β are chosen to be ± 1. The NLS equation is said be *focusing* or *attractive* in the x-dimension if $\alpha > 0$. If $\alpha < 0$, NLS is said to be *defocusing* or *repulsive* in the x-dimension. Similarly, the sign of β will lead to focusing or defocusing in the y-dimension [17]. The NLS equation is called *hyperbolic* if $\alpha\beta < 0$ and *elliptic* if $\alpha\beta > 0$.

The phase contribution $\theta(x)$ of (3b) implicitly depends on α and B in both (3a) and (3d). In order for ϕ and θ to be real-valued functions, we need $B \in [2k^2, 2]$ if $\alpha = 1$ or $B \leq 0$ if $\alpha = -1$. Figure 1 represents the (k, B)-parameter space corresponding to nontrivial phase solutions of NLS. As the phase component θ approaches zero, the solutions approach one of five simpler types of solutions; (*i*) a Stokes wave, (*ii*) a cn solution, (*iii*) a dn solution, (*iv*) a sn solution, (*v*) a soliton-type solutions. Details about the Jacobi elliptic functions sn,cn and dn may be found in [1]. The boundaries of the regions in Fig. 1 correspond to each of these solutions. Table 3.2 summarizes the parameter values for which the NTP solutions reduce to the simpler solutions.

While both TP and NTP solutions are of interest, TP results are reasonably well represented in the literature; for example, see [19, 7, 5, 10, 12, 4, 16, 15], although much of this attention has been focused on the stability of solitary wave solutions. The NTP limits will provide a reference for later discussion, when we refer to the stokes, sn, cn and dn type solutions. We know of few published stability results in the NTP setting [9]. To a large extent this is due to the additional complexity of the linear stability analysis of the NTP solutions, and to the large parameter space that needs to be explored. In this paper, we investigate the spectral stability of all NTP solutions (2), for all possible choices of α and β.

2 The linearized stability problem

In order to study the linear stability of NTP solutions of the NLS equation, we consider perturbations of the form

$$\psi_{_p}(x,y,t) = (\phi(x) + \epsilon u(x,y,t) + i\epsilon v(x,y,t) + \mathcal{O}(\epsilon^2))\mathrm{e}^{i\theta(x)+i\lambda t}, \tag{4}$$

where $u(x,y,t)$ and $v(x,y,t)$ are real-valued functions, ϵ is a small real parameter and $\phi(x)\mathrm{e}^{i\theta(x)+i\lambda t}$ is a NTP solution of NLS. Substituting (4) into (1), linearizing and separating real and imaginary parts leads to

$$\lambda u - 3\gamma\phi^2 u - \beta u_{yy} + \alpha c^2 \frac{1}{\phi^4} u - 2\alpha c \frac{1}{\phi^3}\phi_x v + 2\alpha c \frac{1}{\phi^2} v_x - \alpha u_{xx} = -v_t, \tag{5a}$$

$$\lambda v - \gamma\phi^2 v - \beta v_{yy} + \alpha c^2 \frac{1}{\phi^4} v + 2\alpha c \frac{1}{\phi^3}\phi_x u - 2\alpha c \frac{1}{\phi^2} u_x - \alpha v_{xx} = u_t. \tag{5b}$$

Since (5) does not depend on y or t explicitly, we assume that $u(x,y,t)$ and $v(x,y,t)$ have the form

$$u(x,y,t) = U(x,\rho,\Omega)\mathrm{e}^{i\rho y+\Omega t} + c.c., \tag{6a}$$

$$v(x,y,t) = V(x,\rho,\Omega)\mathrm{e}^{i\rho y+\Omega t} + c.c., \tag{6b}$$

where ρ, is a real constant, $U(x)$ and $V(x)$ are complex-valued functions, Ω is a complex constant and *c.c.* denotes complex conjugate. Notice that ρ is the wavenumber of the transverse perturbation and Ω is the exponential growth constant associated with ρ.

If a bounded U, V exist such that Ω has a positive real part, then the amplitudes of the perturbations grow exponentially in time and the unperturbed solution is said to be unstable. Upon substitution, (5) gives

$$\lambda U - 3\gamma\phi^2 U + \beta\rho^2 U + \alpha c^2 \frac{1}{\phi^4} U - 2\alpha c \frac{1}{\phi^3}\phi_x V + 2\alpha c \frac{1}{\phi^2} V_x - \alpha U_{xx} = -\Omega V, \tag{7a}$$

$$\lambda V - \gamma\phi^2 V + \beta\rho^2 V + \alpha c^2 \frac{1}{\phi^4} V + 2\alpha c \frac{1}{\phi^3}\phi_x U - 2\alpha c \frac{1}{\phi^2} U_x - \alpha V_{xx} = \Omega U. \tag{7b}$$

If $c = 0$, then 7 reduces to the stability analysis of trivial phase solutions. This case is examined in [5, 4, 9, 2, 18, 13] and others. With the linear system (**??**) constructed, we are now able to investigate the stability of the perturbed NTP solution numerically.

3 Numerics

The main problem for the numerical investigation of (7) is the size of the parameter space involved. For every choice of α, β and equation parameters k and B the spectrum of (7) needs to computed for a range of ρ values to determine stability or to analyze any instabilities. To this end, the efficiency of the numerical method is absolutely crucial. The exponential convergence of Hill's method and its black-box implementation, demonstrated in [6], allows for the systematic exploration of the large phase space encountered here.

3.1 Method

To apply Hill's method, Fourier expansions are needed for all coefficients of (7), as well expansions of the unknown functions U and V. The coefficients are written in the complex Fourier form as

$$\begin{aligned} \phi^2 &= \sum_{k=-\infty}^{\infty} Q_k e^{i2k\pi x/L}, & \phi^{-2} &= \sum_{k=-\infty}^{\infty} R_k e^{i2k\pi x/L}, \\ \phi^{-4} &= \sum_{k=-\infty}^{\infty} S_k e^{i2k\pi x/L}, \quad \text{and} & \phi^{-3}\partial_x\phi &= \sum_{k=-\infty}^{\infty} T_k e^{i2k\pi x/L}, \end{aligned} \tag{8}$$

where the values Q_k, R_k, S_k and T_k may be computed with arbitrary precision using a high-order quadrature scheme. Note that since ϕ is even with period L, ϕ^2 is even with period $L/2$. Also, ϕ is never zero except in the limit cases.

The periodicity of the coefficients containing powers of ϕ allows us to decompose the eigenfunctions of U and V of the spectral problem in a Fourier-Floquet form

$$U(x) := e^{i\mu x} \sum_{l=-\infty}^{\infty} U_l e^{-i2l\pi x/PL} \quad \text{and} \quad V(x) := e^{i\mu x} \sum_{l=-\infty}^{\infty} V_l e^{-i2l\pi x/PL}. \tag{9}$$

Here μ is the Floquet parameter and P is introduced for convenience. Allowing μ to be different from 0 admits solutions with periodicity other than $L/2$. We fix $P = 2$, which allows both periodic and anti-periodic eigenfunctions to be considered. The form of U and V in (9) follows from Floquet's theorem and the observation that we seek eigenfunctions which are bounded. Again, see [6] for a more complete explanation.

Substitution of (8) and (9) into (7) allows us to write equations for U_n and V_n as a coupled bi-infinite system of difference equations given by

$$\begin{aligned} -\left(\lambda + \beta\rho^2 - \alpha\left(i\mu + \frac{in\pi}{L}\right)^2\right) U_n + 3\gamma \sum_{k=-\infty}^{\infty} Q_{\frac{n-k}{2}} U_k - \alpha c^2 \sum_{k=-\infty}^{\infty} S_{\frac{n-k}{2}} U_k \\ + 2\alpha c \sum_{k=-\infty}^{\infty} T_{\frac{n-k}{2}} V_k - 2\alpha c\left(i\mu + \frac{in\pi}{L}\right) \sum_{k=-\infty}^{\infty} R_{\frac{n-k}{2}} V_k = \Omega V_n \end{aligned} \tag{10a}$$

$$\left(\lambda+\beta\rho^2-\alpha\left(i\mu+\frac{in\pi}{L}\right)^2\right)V_n-\gamma\sum_{k=-\infty}^{\infty}Q_{\frac{n-k}{2}}V_k+\alpha c^2\sum_{k=-\infty}^{\infty}S_{\frac{n-k}{2}}V_k$$
$$+2\alpha c\sum_{k=-\infty}^{\infty}T_{\frac{n-k}{2}}U_k-2\alpha c\left(i\mu+\frac{in\pi}{L}\right)\sum_{k=-\infty}^{\infty}R_{\frac{n-k}{2}}U_k=\Omega U_n, \quad \text{(10b)}$$

which hold for all integer n. Here $\mu\in[\frac{-\pi}{2K},\frac{\pi}{2K})$ and $Q_{\frac{n-k}{2}}=0$ if $\frac{n-k}{2}\notin\mathbb{Z}$, with R,S and T similarly defined. Equations (10a) and (10b) are *equivalent* to the original system (7) if the Fourier coefficients are exact.

In practice, a pre-multiplication of the linear system by ϕ^4 allows an exact cosine series expansion of ϕ^2,ϕ^4 and ϕ^6 to be used. This follows from the differential equations for $\mathrm{sn}\,(x,k)$ and Jacobi's [11] series expansion of $\mathrm{sn}^2(x,k)$. This pre-multiplication transforms the original eigenvalue problem into a generalized eigenvalue problem. Golub and Van Loan [8] provide a brief discussion of generalized eigenvalue problems. For details of the numerical technique, see [14].

3.2 Experiments

Equations (10a) and (10b) form the foundation for the numerical experiments. By truncating the exact bi-infinite system (10) we can explicitly construct and compute the eigenvalues of a finite dimensional matrix approximation. We consider all four cases: *(I)* defocusing in x with focusing perturbation in y ($-\alpha=\beta=1$), *(II)* defocusing in x with defocusing perturbation in y ($-\alpha=-\beta=1$), *(III)* focusing in x with focusing perturbation in y ($\alpha=\beta=1$), and finally *(IV)* focusing in x with defocusing perturbation in y ($\alpha=-\beta=1$).

In each case, a large number of parameter values in the two dimensional parameter space shown in Fig. 1 were explored numerically. Approximately 5.2 million generalized eigenvalue problems were considered, the size of each determined by the cutoff mode N of the underlying Fourier series. A truncation to N positive Fourier coefficients reduces the bi-infinite exact system (10) to an approximate $(4N+2)$ dimensional problem. The value of N as a function of (k,B) was chosen by computing sample problems over various k's and B's in the parameter region for increasingly large N until the eigenvalues converged to within a measured tolerance. A simple polynomial was then used to fit this data. This information, and details related to other parameter ranges used in the experiments, are included in Tbl. 2. In the table, k is the elliptic modulus, B may be interpreted as a measure of the nontrivial phase quantity θ, $4N+2$ is the matrix dimension used to approximate the full operator, ρ is the wavenumber of the perturbation in the y-dimension, and μ is the Floquet parameter. Also, `linspace(a,b,m)` is a linearly spaced vector from a to b of length m, `logspace(a,b,m)` is a logarithmically spaced vector from 10^a to 10^b of length m and function `ceil(x)` is the smallest integer not less than x.

3.3 Results

First and foremost, it should be stated that *none* of the solutions considered here were found to be spectrally stable. This establishes, at least numerically, that *all* traveling-wave solutions of NLS are unstable. At this point, it remains to investigate the nature of the instabilities, so as to better understand the dynamics of this important class of solutions of the NLS equation.

Using the Fourier-Floquet-Hill method we numerically considered the instabilities due to transverse perturbations with wavenumber denoted by ρ over the range of parameter values of table 2

Parameter	Description	value
k	Elliptic Modulus	$\texttt{linspace(0,1,65)}$
B	Shift	For $\alpha = -1 : -\texttt{logspace}(-8, 0, 65)$ For $\alpha = \quad 1 : (2k^2 + \texttt{logspace}(-8, 0, 65)) \cap (2k^2, 2)$
N	Fourier cutoff	For $\alpha = -1 : 15 + \texttt{ceil}(5\texttt{k}^5)$ For $\alpha = \quad 1 : 10 + \texttt{ceil}(25\texttt{k}^{10})$
ρ	perturbation wavenumber	$\texttt{linspace(0,4,65)}$
μ	Floquet parameter	$\texttt{linspace}(-\frac{\pi}{2\texttt{K}}, \frac{\pi}{2\texttt{K}}, 21)$

Table 2: Parameter values and ranges used in numerical experiments.

and the one-dimensional ($\rho = 0$). Each experiment consisted of computing the eigenvalues of the generalized eigenvalue problem. For each parameter triplet (k, B, ρ), for $\alpha, \beta = \pm 1$, a sequence of Floquet parameters μ was chosen from the interval $[\frac{-\pi}{2L}, \frac{\pi}{2L}]$. The generalized eigenvalues and eigenvectors were computed from the resulting matrix. The generalized eigenvalues are approximations of spectral elements of (7), and an approximation of the corresponding eigenfunctions may be easily reconstituted from the generalized eigenvectors.

Since a single eigenvalue with positive real part will lead to instability of the system, the eigenvalue with largest real part over all choices of μ was recorded for each (k, B, ρ) triplet. That is, we compute

$$\Omega_{growth}(k, B, \rho) = \max_{\mu \in [-\pi/2L, \pi/2L]} (Re(\Omega(k, B, \rho, \mu))),$$

which we call the growth rate. We reduce the dimension still further by computing the largest such instability over all sampled perturbation wave numbers ρ. This quantity,

$$\Omega_{\max}(k, B) = \max_{\rho \in [0,4]} (\Omega_{growth}),$$

the maximal growth rate, is plotted in the first column of figure 3.3.5. This represents the maximal exponential growth rate a solution with parameters (k, B) can undergo, and allows us to determine the solution which is spectrally the least unstable. We also recorded the minimum growth rate that a solution should experience,

$$\Omega_{\min}(k, B) = \min_{\rho \in [0,4]} (\Omega_{growth}),$$

to verify that all solutions experience positive real exponential growth. We note the maximum over (k, B) of the maximal growth rate as well as the minimum over (k, B) of the minimal growth rate in the first column of Fig. 3.3.5.

Before we can discuss the plots of Fig. 3.3.5, the vertical axis requires some explanation. In plots *I* and *II*, the $1-1$ transform $T_f(B) = (B - 2k^2)/(2 - 2k^2)$ is used to normalize the range of B. This maps the interval $[2k^2, 2]$ to $[0, 1]$. The transform $T_d(B) = -B$ is used in *III* and *IV*. In both cases, these $1 - 1$ transformations scale the interval containing B to the unit interval [0,1]. Every point in Fig. 3.3.5 corresponds to a solution, and the boundaries in the figure are the boundaries of the regions represented in Fig. 1. In all cases, we present the plots using a $\log_{10}$ scale of the vertical dimension.

The column on the right of Fig. 3.3.5 indicates the wave number ρ which leads to maximal growth. Recall that our computations were truncated at $\rho = 4$, and so an observed value of $\rho = 4$

indicates that there is a strong short-wavelength(large ρ) instability. The first two rows of Fig. 3.3.5 correspond the x-focusing parameter range $(k, B) = (0, 1) \times (2k^2, 2)$ in the $\alpha = 1$ case of Fig. 1(a), while the last two rows correspond to the x-defocusing parameter range of $(k, B) = (0, 1) \times (-1, 0)$ shown in Fig. 1(b).

3.3.1 Case *I*: $\alpha = \beta = 1$

The plots *I*(a) and *I*(b) of Fig. 3.3.5 summarize the computed instabilities in the case of focusing in both the x- and y -dimensions. This setting is applicable to nearly monochromatic waves of small amplitude in pulse propagation in optical waves. This is the setting which limits to the bright solitons for $k = 1$. Recall that the original parameter space corresponds to $(k, B) = (0, 1) \times (2K^2, 2)$, and that the map T_f is used to transform this to $(0, 1) \times (0, 1)$. This transform, coupled with the $\log_{10}$ scaling, causes the plots to become increasingly sparse towards the right bottom corner.

A distinct ridge of large instability is noticeable in the growth plot *I*(a). The ridge appears to begin near the trivial limit $k = 0$ and $B = 0$, and remains close to the cn limit boundary (within approximately .02 units) as k increases, to reach first a local minima near $k = 0.7$ and then a global minimum near $k = 0.96$. The growth plot *I*(a) also indicates that system stability factor grows quickly for fixed k as B moves away from the cn TP solution at the bottom the plot. After this point, increasing B causes the growth factor to decrease, although this time more slowly, as the dn TP solution is aproached at the top edge of the plot. This suggests that for fixed k, the cn-type solution loses stability much more quickly (in this parameter space) than does a corresponding dn-type solution. In comparison, for fixed B, the stability increases more slowly as k varies from 0 to 1.

In *I*(b), the wavelength corresponding to the maximal growth of *I*(a) are given. In this case, the maximum instability occurs for the shortest wavelength samples, although there appears to be a possible periodicity in the region where k is larger than about 0.95. The periodicity is more noticeable in the $\alpha = -\beta = 1$ setting, and will be discussed in the next section.

3.3.2 Case *II*: $\alpha = -\beta = 1$

Plots *II*(a) and *II*(b) of Fig. 3.3.5 summarize the computed instabilities in the case of focusing in the x-dimension and defocusing in the y-dimension. Although this case is considered as a deep water waves rather then optical pulses, the same general stability comments of Case *I*(a) are applicable here. Notice that both the maximum and minimum growth rates are slight larger in this setting than in the the previous one. Also, the maximum R_max appears to be located near a saddle centered roughly at $(0.7, -2)$, as was the maximum of *I*(a).

A banding structure is evident in plot *II*(b), both in the horizontal banding in the upper section and the vertical banding at the bottom and also the bottom left portions. The growth factor appears constant, but the corresponding wave number appears to sweep through a distinct range of ρ values.

3.3.3 Case *III*: $-\alpha = \beta = 1$

Plots *III*(a) and *III*(b) of Fig. 3.3.5 summarize the computed instabilities in the case of defocusing in the x-dimension and focusing y-dimension. These plots again correspond to the deep water setting.

A distinct ridge of large instability is noticeable in the growth plot *III*(a). The ridge appears to begin near the trivial limit $k = 0$ and $B = 0$, and remains close to the sn limit boundary (within approximately .02 units) as k increases, to reach a global maximum near $k = 0.02$ and $B = -0.0001$. The ridge then appears to decrease in amplitude as k increases towards 1. For solutions near the Stokes wave limit, $k = 0$, the solutions appear to lose stability quickly as k increases, but that an increase in B will delay this process. The increase in the growth rate is most rapid near the sn-type solution limit at $B = 0$.

We remark that while the plot *III*(a) is quite similar to *II*(a), the (k, B)-parameter space is much different in this setting. The maximum exponential growth rate occurs for k near the Stokes wave boundary of $k = 0$.

3.3.4 Case *IV*: $-\alpha = -\beta = 1$

The plots *IV*(a) and *IV*(b) of Fig. 3.3.5 summarize the computed instabilities in the case of defocusing in both the x- and y-dimensions. As in *I*, this setting is applicable to nearly monochromatic waves of small amplitude in pulse propagation in optical waves. For $B = 0$, sn-type solutions exist and grey solitons occur in the limit $k = 1$. We omit a general description of the surface as the stability plot *IV*(a) is nearly identical to that of *III*(a).

In *IV*(b) the wavelengths corresponding to the maximal growth of *I*(a) are plotted. Although *III*(a) and *IV*(a) are similar, the plots of corresponding wave numbers given by *III*(b) and *IV*(b) are very different. It appears that a majority of the maximal instability is attributable to small ρ (long wave) perturbations. In fact, the largest growth occurs for $\rho = 0$.

3.3.5 Comparisons

Perhaps most notable in a comparison of the growth stability plots of Fig. 3.3.5 is the observation that the stability surfaces are qualitatively very similar in all cases, and that the growth factor does not grow appear to grow monotonically for any fixed choice of $k \in (0, 1)$. Instead, the maximal growth rate is achieved at some point in the interior of the admissible (k, B)-parameter space. There are other evident relationships. The overall qualitative structure of the growth surface is quite similar in both the focusing case *I-II*(a) and in the defocusing case *III-IV*(a), suggesting that α may be used to distinguish these surfaces. The position of both the maxima and minima appear to be influenced only slightly by the sign of the perturbation, both for $\alpha = 1$ and when $\alpha = -1$. When $\alpha = 1$, case *I-II*, the largest instability is achieved for relatively large values of k, in contrast the location of the maximal growth of $\alpha = -1$ in *III-IV*, which occurs for relatively small values of k, and is located near the stokes trivial phase limiting case. Also, the distinct local nature of the maxima in the $\alpha = 1$ of cases *I-II*(a) is different from the more global nature of the maxima in the $\alpha = -1$ *III-IV*(a) setting. We also note that in all cases the minimum growth rate is found nearest to the stokes limit of $k = 0$, and that the stability values are slightly larger in the hyperbolic setting *II-III*(a) when compared to the elliptic setting *I,IV*(a).

4 Summary

In this paper, we considered the spectral instability of one-dimensional traveling wave NTP solutions of the cubic Nonlinear Schrödinger equation. The solutions used are based on Jacobi elliptic

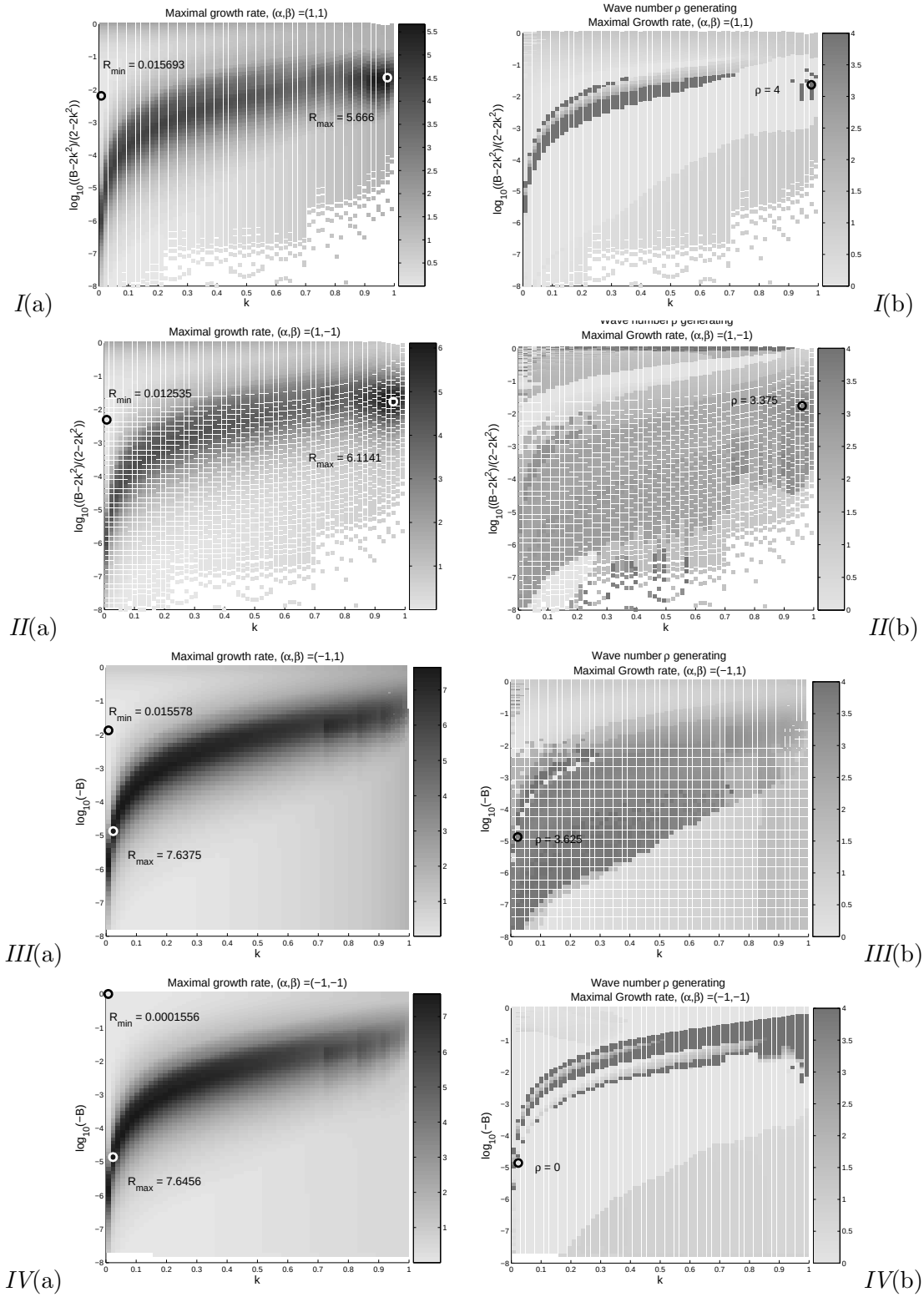

I(a) *I*(b)

II(a) *II*(b)

III(a) *III*(b)

IV(a) *IV*(b)

Figure 2: Plots representing (a) maximum spectral growth for $\rho \in [0, 4]$ and (b) indicating corresponding wave number leading to instability. Here $R_{\max} = \max_{k,B,\rho}(\max_{\mu}(Re(\Omega)))$ and $R_{\min} = \min_{k,B,\rho}(\max_{\mu}(Re(\Omega)))$. The vertical axis is on a $\log_{10}$ scale.

function with transverse perturbation. And exact spectral form of the linearized operator is discretized and used to construct an associated eigenvalue problem. The positive real part of the resulting eigenvalues were then used to determine that *none* of the solutions considered are spectrally stable. The numerics indicate a well defined ridge of maximal instability which is located in the (k, B)-parameter region associated with fully nontrivial phase solutions. In addition, the numerical evidence indicates that exponential growth rates of dn-type solutions, and to a lesser extent the Stokes wave solutions, are robust under transverse perturbation. The growth of the cn-type and sn-type solutions appear to be quite sensitive to this perturbation. In summary, numerical evidence suggests that bounded, nontrivial one dimensional traveling wave solutions to the cubic NLS equation are unstable under transverse perturbation.

References

[1] M. Abramowitz and I.A. Stegun. *Handbook of mathematical functions*. National Bureau of Standards, Washington D.C., 1974.

[2] V. A. Aleshkevich, *et al.* . Stability of spatiotemporal cnoidal waves in cubic nonlinear media. *Phys Rev E*, 67:066605, 2003.

[3] P. F. Byrd and M. D. Friedman. *Handbook of Elliptic Integrals for Engineers and Physicists*. Springer-Verlag, 1954.

[4] J. Carter and B. Deconinck. Stability of trivial phase solutions fo the two-dimensional cubic nonlinear schrödinger equation. *in preparation*, 2005.

[5] J. Carter and H. Segur. Instability in the two-dimensional cubic nonlinear schrödinger equation. *Phys. Rev. E.*, 68(4):#045601, 2003.

[6] B. Deconinck and J. N. Kutz. Computing spectra of linear operators using Hill's method. *in preparation*, 2005.

[7] A.M. Rubenchik E.A. Kuznetsov and V.E. Zakharov. Soliton stability in plasmas and hydrodynamics. *Phys. Rep.*, 142:103–165, 1986.

[8] G. H. Golub and C. F. Van Loan. *Matrix Computations*. Johns Hopkins University Press, 1996.

[9] E. Infeld and J. Ziemkiewicz. Stability of complex solutions of the nonlinear schrödinger equation. *Acta Phys Pol*, A59(3):255, 1981.

[10] B. Deconinck J. Carter and D. E. Pelinovsky. Transverse instabilities of deep-water solitary waves. *in preparation*, 2005.

[11] C. G. Jacobi. *Fundamenta Nova Theoriae Functionum Ellipticarum*. Königsberg, 1829.

[12] Y. S. Kivshar and D. E. Pelinovsky. Self-focusing and transverse instabilities of solitary waves. *Phys Rep*, 331(4):118–195, 2000.

[13] D. U. Martin, H. C. Yuen, and P. G. Saffman. Stability of plane wave solutions o fthe two-space-dimensional nonlinear schrödinger equation. *Wave Motion*, 2:215–229, 1980.

[14] C. Moler and G.W. Stewert. An algorithm for generalized matrix eigenvalue problem. *SIAM J. Numer. Anal.*, 10(2), 1973.

[15] K. Rypdal and J. J. Rasmussen. Stability of solitary structures in the noninear schrödinger equation. *Physica Scripta*, 40:192, 1989.

[16] G. M. Fraiman S. E. Fil'chenkov and A. D. Yunakovskii. Instability of periodic solutions of the nonlinear schrödinger equation. *Sov. J. Plasma Phys.*, 18(8):961–966, 1987.

[17] P. L. Sulem and C. Sulem. *Nonlinear Schrödinger Equations: Self-focusing and Wave Collapse.* Springer-Verlag, NY, 1999.

[18] V.A. Aleshkevich, V.A. Vysloukh, A.A. Egorov and A.S. Zelenina Y. V. Kartashov. Transverse modulational instability of (2+1)-dimensional cnoidal waves in media with cubic nonlinearity. *J Opt Soc Am B*, 20(6):1273–1284, 2003.

[19] V. E. Zakharov and A. M. Rubenchik. Instability if waveguides and solition in nonlinear media. *Sov Phys JETP*, 38(3):494–500, 1974.